

---

# LEARNING ANY-VIEW 6DOF ROBOTIC GRASPING IN CLUTTERED SCENES VIA NEURAL SURFACE RENDERING

---

PREPRINT

Snehal Jauhri<sup>1</sup>, Ishikaa Lunawat<sup>2,†</sup>, and Georgia Chalvatzaki<sup>1,3,4</sup>

<sup>1</sup> Computer Science Department, Technische Universität Darmstadt, Germany

<sup>2</sup> NIT Trichy, India

<sup>3</sup> Hessian.AI, Darmstadt, Germany

<sup>4</sup> Center for Mind, Brain and Behavior, Uni. Marburg and JLU Giessen, Germany

† Work done during internship at Technische Universität Darmstadt, Germany

snehal.jauhri@tu-darmstadt.de

ishikaa.nitt@gmail.com

georgia.chalvatzaki@tu-darmstadt.de

## ABSTRACT

Robotic manipulation is critical for admitting robotic agents to various application domains, like intelligent assistance. A major challenge therein is the effective 6DoF grasping of objects in cluttered environments from any viewpoint without requiring additional scene exploration. We introduce *NeuGraspNet*, a novel method for 6DoF grasp detection that leverages recent advances in neural volumetric representations and surface rendering. Our approach learns both global (scene-level) and local (grasp-level) neural surface representations, enabling effective and fully implicit 6DoF grasp quality prediction, even in unseen parts of the scene. Further, we reinterpret grasping as a local neural surface rendering problem, allowing the model to encode the interaction between the robot’s end-effector and the object’s surface geometry. *NeuGraspNet* operates on single viewpoints and can sample grasp candidates in occluded scenes, outperforming existing implicit and semi-implicit baseline methods in the literature. We demonstrate the real-world applicability of *NeuGraspNet* with a mobile manipulator robot, grasping in open spaces with clutter by rendering the scene, reasoning about graspable areas of different objects, and selecting grasps likely to succeed without colliding with the environment. Visit our project website: <https://sites.google.com/view/neugraspnet>.

## 1 Introduction

Robotic manipulation is crucial in various applications, like industrial automation, assistive robots, etc. A key component for manipulation is effective 6DoF grasping in cluttered environments, as this ability would enhance the efficiency, versatility, and autonomy of robotic systems operating in unstructured environments. Grasping effectively with limited sensory input reduces the need for extensive exploration and multiple viewpoints, enabling efficient and time-saving solutions to robotic applications. Robotic grasping involves generating suitable poses for the robot’s end-effector given some sensory information (e.g., visual data). While planar bin picking, i.e., top-down 4DoF grasping (3D position and roll orientation) with two-fingered or suction grippers, has mainly been solved thanks to deep learning models [1–4], 6DoF grasping in the wild, i.e., grasping in the  $SE(3)$  space of 3D positions and 3D rotations from any viewpoint remains a challenge [5, 6]. Embodied AI agents, e.g., mobile manipulation robots [7, 8], are expected to perform manipulation tasks similar to humans; humans can leverage geometric information from limited views and mental models to grasp objects without exploring to reconstruct the scene. Such an elaborate plan for grasping in open spaces with clutter would require that robots, given some spatial sensory information, e.g., 3D pointcloud data, can reconstruct the scene, understand the graspable area of different objects, and finally select grasps that are highly likely to succeed, both in terms of lifting an object for a subsequent manipulation task, but crucially, without colliding and potentially damaging the surrounding environment.

Existing 6DoF grasping methods try either to generate explicitly feasible grasp poses [9–12] on partial pointclouds or implicitly classify grasp quality of grasp samples [13–15]. A comprehensive review on deep grasp synthesis is introduced in [6]. We refer to a subset of works covering explicit grasp generative models, implicit (discriminative models) and semi-implicit methods in appendix D. Crucially, the ability to assess grasp quality implicitly is essential to many applications in which, due to human demonstrations [16] or other affordance-based information [17] 6DoF grasp candidates may be pre-defined. Another benefit of implicit grasp functions is their ability to be combined with additional constraints regarding specific affordances in a scene [18], e.g., using such implicit functions as cost functions for grasping optimization [19, 20]. Nevertheless, many existing methods that generate grasp candidates using partial pointclouds either rely only on the perceived regions of a scene [21, 12] or accumulate more information from multiple views [22–24]. A reasonable approach to mitigate partial observability from pointclouds is to learn neural scene representations [25–27] to learn to complete scenes in the continuous functional space to render surfaces and volumes of objects [28–30]. Their implicit nature enables querying the geometry of any arbitrary point in the scene, making them an attractive solution for robotic grasping [31–33].

This work investigates how to effectively leverage geometric and surface information about objects in scenes perceived from *any partial view* to detect high-fidelity 6DoF grasps. We propose a novel method for 6DoF grasp detection building on advances in neural geometric representations [26, 25] and surface rendering [34, 29], to further highlight and extend their applicability to practical problems like robotic manipulation. While semi-implicit methods [31] have leveraged joint training on scene reconstruction and grasp prediction, they have *yet to explicitly* use valuable information from the reconstructed scenes. We present a new method that learns both global (scene-level) and local (grasp-level) neural surface representations for effective and *fully implicit* 6DoF grasp quality prediction.

Our method learns an implicit scene representation that reconstructs parts of the scene that are invisible, allowing us to render the scene and generate and evaluate grasp candidates even in unseen parts from *any* single-camera viewpoint. Moreover, we argue that the local geometric object information is essential for understanding the complementarity between the robotic end-effector and the object’s surface for predicting grasp success. For that, we view *grasping as local neural surface rendering* for learning local representations that encode the response of an object part to a respective grasping pose. We call our method *NeuGraspNet*<sup>1</sup> to highlight the importance of global and local neural representations in detecting high-fidelity grasp poses in challenging cluttered scenes from any viewpoint. To evince the benefit of our method, we show superior performance compared to implicit and semi-implicit baselines from the literature in simulated environments. Notably, we demonstrate the real-world applicability of NeuGraspNet with a mobile manipulator robot grasping in clutter.

To summarize, our **contributions** are (i) a new neural grasping quality network (NeuGraspNet) that can operate on **single viewpoints** of a scene and is **fully implicit** in SE(3) and in scene/object geometry; (ii) a new structured method for **sampling grasp candidates in unseen parts of the scene** leveraging global (scene-level) rendering; (iii) the re-interpretation of **grasping as surface rendering** for extracting *local geometric information and features* that capture well the interaction between the robot’s end-effector and the local object-geometry per grasp candidate.

## 2 Background

### 2.1 Problem description

In a cluttered scene with  $M$  objects placed on a support surface, we are given a 3D pointcloud of  $N$  points  $\mathbf{x} \in \mathbb{R}^3$  captured by a depth camera. The camera is pointed towards the objects but can be placed at an arbitrary viewing angle and distance, i.e., the viewpoint is on the  $S^2$  sphere with an arbitrary sphere radius  $\mathbf{rad} \in \mathbb{R}$ . Most grasping methods consider a robot equipped with a two-fingered gripper. Formally, a grasp pose  $\mathbf{g} \in \mathbb{R}^6$  can be represented as an approaching 6-dimensional vector (3D positions and orientations) in the SE(3) space from the center of the robotic gripper’s center to a point on the surface of an object. Thus, 6DoF grasping can be defined as the problem of using the scene information  $\mathbf{x}$  to detect SE(3) grasp poses  $\mathbf{g}$  likely to achieve grasp success. The likelihood of success of a grasp is interpreted as the grasp’s quality  $q \in [0, 1]$ .

### 2.2 Convolutional Occupancy Networks

Convolutional Occupancy Networks (ConvONets) [26] are implicit neural representations for learning-based 3D scene reconstruction. Given a pointcloud  $\mathbf{x}$  or 3D voxel grid of the scene, ConvONet encodes the scene in a feature space  $\psi(\mathbf{x})$  using convolutional encoders which combine global and local scene information. For a query 3D point

<sup>1</sup>The acronym hints at the novel view of grasping as neural surface rendering, but is also a wordplay for the German word ‘neu’ that means new.

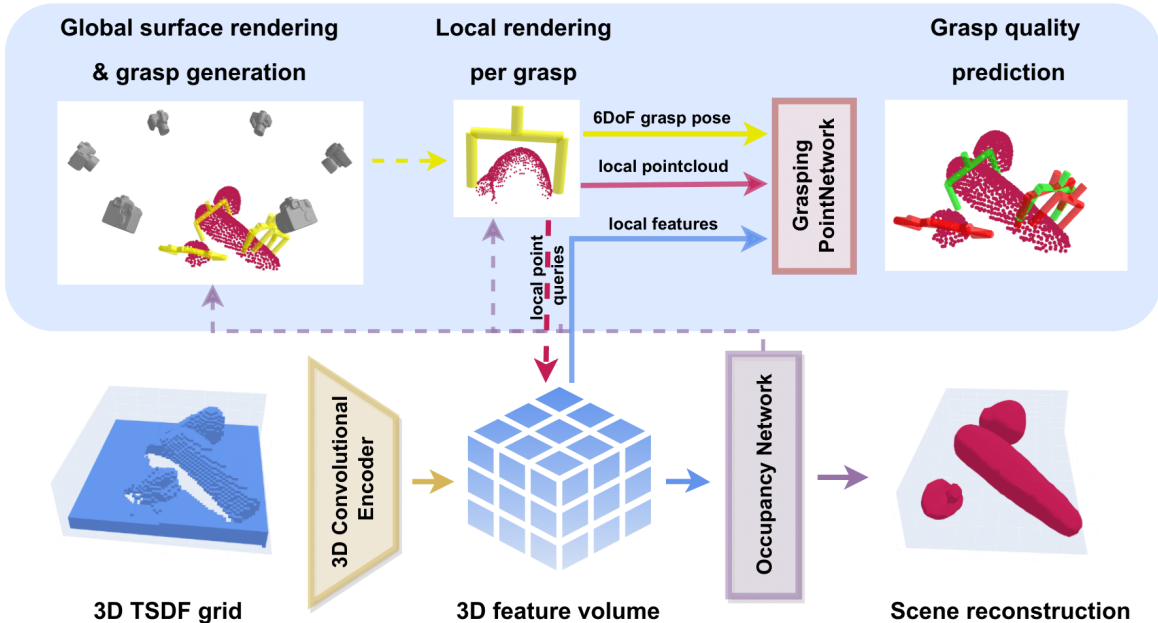


Figure 1: *NeuGraspNet*: A 3D Truncated Signed Distance Field (TSDF) grid is processed through a convolutional occupancy network to reconstruct the scene (cf. section 3.1). The occupancy network is used to perform global, scene-level rendering. The rendered scene is used for grasp candidate generation in  $SE(3)$  (cf. section 3.2). We reimagine *grasping as rendering* of local object-pointclouds and query their features from the 3D feature volume of the convolutional encoder. Local points, their features, and the 6DoF grasp pose are passed to a PointNetwork to predict per grasp quality (cf. section 3.3). *NeuGraspNet* effectively learns the interaction between the objects’ geometry and the gripper to detect high-fidelity grasps. Highlighted in light blue is our core contribution.

$\mathbf{p} \in \mathbb{R}^3$ , it then predicts the probability of the point  $\mathbf{p}$  being occupied using the corresponding feature vector  $\psi(\mathbf{x}, \mathbf{p})$ . The feature vector is passed through a decoder  $f_\theta$  with a sigmoid at the output leading to the occupancy prediction  $o(\mathbf{p}) = f_\theta(\psi(\mathbf{x}, \mathbf{p})) \rightarrow [0, 1]$ . ConvONets combine convolutional encoders with implicit occupancy decoders, effectively leveraging spatial inductive biases, i.e., exploiting the global feature representation capability of CNNs and the fine-grained local geometric modeling capacity of occupancy networks [25].

### 2.3 Surface Rendering

Neural surface rendering approaches [34, 29, 28] employ learned implicit geometric representations, such as occupancy networks [25] or surface models [27, 28], to render realistic 3D object surfaces. While some learned geometric representations require explicit 3D supervision [25, 27, 26], advances in neural radiance fields [35] and surface model learning have also enabled the reconstruction of accurate geometry from multi-view 2D images only [34, 28]. Given any implicit geometric representation that can predict the occupancy probability  $o(\mathbf{p}) \in [0, 1]$  of a point  $\mathbf{p}$  in the scene, the surface is implicitly determined by the level set  $o(\mathbf{p}) = 0.5$ , i.e., the transition between occupied and unoccupied space. The surface points can be extracted at an arbitrary resolution using either isosurface extraction techniques [25] or by ray-marching from a virtual camera pose [34, 29].

## 3 Learning 6DoF Grasping via Neural Surface Rendering

Our goal is to enable a robot equipped with a two-fingered gripper to detect and execute viable 6DoF grasps in cluttered scenes. Scene information is passed to the robot as a pointcloud captured by a depth camera with a random viewpoint, which is the norm when using a robot-embodied camera (cf. fig. 4). For such a setting (cf. section 2.1), we aim to learn an implicit function  $f_\theta^{sg} : \mathbb{R}^3 \rightarrow \mathbb{R}$  that represents the *scene geometry* and a subsequent implicit function  $h_\omega^g : \mathbb{R}^6 \rightarrow \mathbb{R}$  that evaluates the *quality of candidate  $SE(3)$  grasp poses* on parts (objects) of the scene ( $\theta$  and  $\omega$  are the trainable network parameters that are trained jointly), leading to a *fully implicit* representation learning problem.

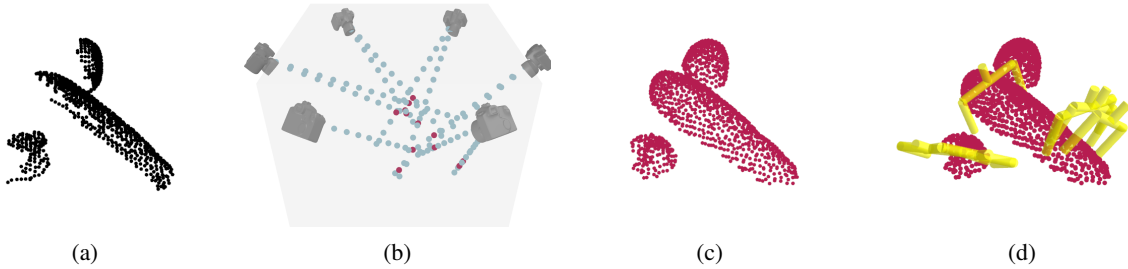


Figure 2: Our scene-level surface rendering approach: (a) an input partial-view pointcloud; (b) surface rendering on the neural implicit geometry (grey volume) using 6 ‘virtual’ cameras; (c) the reconstructed surface pointcloud; (d) grasp candidates sampled on the completed surface.

In the following, we describe our novel method *NeuGraspNet* that combines neural geometric representation learning for scene reconstruction and rendering together with geometric grasp sampling to learn a quality function. The full pipeline is depicted in Fig. 1. We first describe our reconstruction and scene-level rendering approach. We then explain the candidate grasp generation method that samples grasps on the rendered scene, followed by explaining our implicit grasp quality prediction approach that uses local grasp-level surface rendering to query appropriate features relevant to each grasp on the objects’ surface. We conclude this section with some implementation details.

### 3.1 Neural scene reconstruction

Since our input pointcloud  $\mathbf{x}$  is captured by a single-view depth camera, it conveys only partial information about the objects in its field of view. To enable grasp generation with more complete information about the scene, we reconstruct the scene through an implicit scene geometry representation. For this, we use a convolutional occupancy network (ConvONet) as described in section 2.2. The network first encodes the input pointcloud  $\mathbf{x}$  into a feature space  $\psi$ . We can then implicitly query the occupancy probability of any 3D point  $\mathbf{p} \in \mathbb{R}^3$  by passing the corresponding feature vector  $\psi(\mathbf{x}, \mathbf{p})$  through the fully-connected scene geometry decoder network  $f_{\theta}^{sg}$ . The network is trained using ground truth occupancy values  $o(\mathbf{p}) \in \{0, 1\}$  of points uniformly sampled in the scenes. Formally, the reconstruction loss is a binary cross-entropy loss between the predicted occupancy probability  $\hat{o}(\mathbf{p}) = f_{\theta}^{sg}(\psi(\mathbf{x}, \mathbf{p}))$  and the true occupancy  $o(\mathbf{p})$ :

$$\mathcal{L}_{occ}(\hat{o}(\mathbf{p}), o(\mathbf{p})) = -[o(\mathbf{p}) \cdot \log(\hat{o}(\mathbf{p})) + (1 - o(\mathbf{p})) \cdot \log(1 - \hat{o}(\mathbf{p}))]. \quad (1)$$

Learning scene geometry as auxiliary task for grasp quality prediction has been shown to be beneficial to grasp prediction [33, 31]. In this work, we adopt this intuitive idea and further highlight the importance of scene reconstruction not only as an auxiliary training task but as a core component of *NeuGraspNet*. Crucially, we use the learned implicit geometry to render the scene surface for two original parts of our method (cf. fig. 1); at a global level for grasp candidate generation (cf. section 3.2), and at a local level for feature extraction per 6D grasp candidate pose (cf. section 3.3). To enable more fine-grained surface rendering that is necessary for predicting grasps on objects, we train *NeuGraspNet* with additional local occupancy supervision, as detailed in section 3.3.

### 3.2 Scene-level surface rendering & grasp candidate generation

Using the learned occupancy representation  $f_{\theta}^{sg}$ , we can render the surface of the whole scene at inference time by ray-marching  $C$  ‘virtual’ cameras placed in a circular path around the scene (fig. 2). We perform surface rendering using a root-finding approach similar to [34] and [29]. Formally, for every ray  $r$  emanating from each of the  $C$  virtual cameras, we evaluate the occupancy network  $f_{\theta}^{sg}(\cdot)$  at  $n$  equally spaced samples on the ray  $\{\mathbf{p}_j^r\}_{j=1}^n$ . The first point along a ray for which the occupancy changes from free space ( $o(\mathbf{p}) < 0.5$ ) to occupied space ( $o(\mathbf{p}) > 0.5$ ) is a surface point  $\mathbf{p}_s$ . To further refine the surface point estimation, we use an iterative secant search method along the ray (detailed in [34]). After obtaining the surface point-set from all virtual cameras, we merge and downsample the point-set to arrive at a reconstructed scene pointcloud  $\{\mathbf{p}_i\}_{i=1}^M$  as shown in Fig. 2.

Our grasp detection method is implicit, which ensures that we can query the quality of any 6DoF grasp pose  $\mathbf{g} \in \mathbb{R}^6$ . To generate suitable grasp-proposals to discriminate upon, we can use any reasonable grasp-generation technique. We propose using the grasp sampling approach of GPG [36] due to its simple yet effective nature. The GPG sampler takes an input pointcloud and generates grasp candidates by using the point surface normals and estimating the axis of curvature of a surface. For more details, we refer the reader to [36]. We apply the GPG sampler on our *reconstructed* surface pointcloud. This provides two benefits over sampling on the partial input pointcloud. First, we can sample more

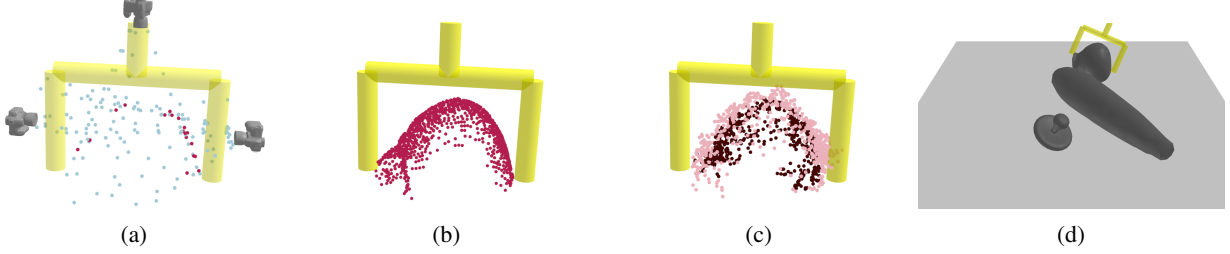


Figure 3: Our local surface rendering approach: (a) surface rendering on the neural implicit geometry by ray-marching three ‘virtual cameras’ that encompass the three parts of the gripper (gripper used here only for visualization); (b) the neural rendered surface; (c) the noisy ground-truth rendered surface used during training for local occupancy supervision (light pink points belong to unoccupied space and dark red points belong to occupied); (d) the ground-truth scene.

grasps since we can use the *completed* scene information, i.e., sample grasps in areas unseen by the camera. Secondly, we can better filter out grasps that collide with the objects in the scene. When sampling on partial pointclouds, proposed candidates may collide or intersect with actual objects. A visualization of the grasps generated on our completed pointcloud can be seen in Fig. 2. Additional comparisons of the plain pointcloud-based GPG and our proposed GPG on rendered scenes can be found in appendix B.

### 3.3 Local surface rendering & grasp quality prediction

A key part of our approach is to learn the appropriate geometric interaction between any 6DoF grasp and the scene. To do this, we propose using features from the scene’s local surface points *rendered* by each grasp. We hypothesize that the local surface points and their corresponding latent features provide the necessary information to effectively encode the geometric complementarity of object-surface and gripper to assess the quality of grasps. For each grasp pose  $\mathbf{g} \in \mathbb{R}^6$  in a scene, we use our implicit scene-geometry network  $f_{\theta}^{sg}$  and our surface rendering approach (section 3.2) to obtain a local 3D surface point set  $\{\mathbf{p}_i^{\mathbf{g}}\}_{i=1}^N$  corresponding to the grasp  $\mathbf{g}$ . Specifically, we place a virtual camera near each link of the gripper, i.e., near the two fingers and the base, such that the cameras point towards the inner hull of the gripper (fig. 3). For this local rendering, we use higher-resolution virtual cameras as compared to the scene-level rendering to obtain a dense local point-set, and we filter out spurious points too far away from the gripper links (cf. appendix A).

To predict the quality of a grasp  $\mathbf{g}$ , we use the local surface point set of the grasp  $\{\mathbf{p}_i^{\mathbf{g}}\}_{i=1}^N$  as well as the corresponding feature vectors of this point set in the *same feature space*  $\psi(\mathbf{x})$  as the scene geometry network  $f_{\theta}^{sg}$ . In this way, we jointly learn features  $\psi$  appropriate for both scene reconstruction and grasp quality prediction, exploiting synergies between them [31]. The  $N$  local surface points and their features are passed through an implicit grasp quality decoder network  $h_{\omega}^g$  to predict the grasp success probability  $\hat{q}(\mathbf{g}) = h_{\omega}^g(\{\mathbf{p}_i^{\mathbf{g}}, \psi(\mathbf{x}, \mathbf{p}_i^{\mathbf{g}})\}_{i=1}^N)$ . To process this *set of points and features per grasp*, the grasp quality decoder uses a permutation invariant point network architecture. Grasp quality is trained using ground truth labels  $q(\mathbf{g}) \in \{0, 1\}$  of grasp success/failure and a binary cross-entropy loss

$$\mathcal{L}_{qual}(\hat{q}(\mathbf{g}), q(\mathbf{g})) = -[q(\mathbf{g}) \cdot \log(\hat{q}(\mathbf{g})) + (1 - q(\mathbf{g})) \cdot \log(1 - \hat{q}(\mathbf{g}))]. \quad (2)$$

**Local supervision using ground truth surface points.** Predicting grasp quality based on surface features poses a challenge. Since we rely on local neural surface point rendering to pick appropriate point-wise features, the scene reconstruction needs to be accurate. A straightforward approach would be to train the grasp quality network  $h_{\omega}^g$  in a subsequent step after the convergence of the scene reconstruction network  $f_{\theta}^{sg}$ . However, we want to train grasp quality and scene reconstruction *jointly* to ensure that the implicit geometric features  $\psi$  also capture information relevant for assessing grasp quality in the challenging SE(3) space. Thus, we propose to use additional local surface supervision at training time. During the data generation phase, we render the ground truth surface points for each grasp:  $\{\mathbf{p}_{gt\ i}^{\mathbf{g}}\}_{i=1}^N$ . We then add noise to these surface points, as visualized in Fig 3(c). These noisy surface points  $\{\mathbf{p}_{noisy\ i}^{\mathbf{g}}\}_{i=1}^N$  serve two purposes. Firstly, we can *train a robust grasp quality network* using these noisy surface points and their features  $\psi$  using the loss from eq. (2). This means that we only need to use the local neural surface rendering at *inference time* while also ensuring regularization against imperfect surface renders. Secondly, we can add additional supervision to the scene reconstruction using the occupancy values for these dense yet noisy surface points  $o(\mathbf{p}_{noisy})$ , which provide a good signal to the scene reconstruction function, refining the occupancy in scene parts that interact with the gripper during grasping (cf. Fig. 3). We use a loss function  $\mathcal{L}_{local}$ , similar to eq. (1), to additionally train *local object-part reconstruction* from those noisy surface points.



### 3.4 Implementation

Our network consists of a convolutional occupancy network encoder that encodes the input pointcloud or Truncated Signed Distance Field (TSDF) into an implicit 3D feature space  $\psi$  with three feature planes [26]. Since we consider our input to originate from a random viewpoint depth camera, an alternate approach could be to also incorporate rotational SO(3) equivariance in our encoder network. Thus, we also experiment with a modified convolutional encoder that first uses a VectorNeuron-PointNet [37] to encode SO(3) equivariant point-wise features and then projects these features into the three feature planes.

For scene reconstruction, the decoder  $f_{\theta}^{sg}$  is a ResNet-based fully-connected network (same as [26]). For grasp quality prediction, the decoder  $h_{\omega}^q$  uses a point network architecture. We experiment with two popular network architectures: PointNet [38] and DGCNN [39].

The overall loss during training includes the occupancy loss  $\mathcal{L}_{occ}$ , quality loss  $\mathcal{L}_{qual}$  as well as the additional local occupancy loss  $\mathcal{L}_{local}$ , each weighted by factors  $w_i$ ,

$$\mathcal{L} = w_0\mathcal{L}_{occ} + w_1\mathcal{L}_{qual} + w_2\mathcal{L}_{local}. \quad (3)$$

A detailed description of the network architecture and additional implementation details are provided in appendix A. In the main paper, we report results from the best-performing architecture of NeuGraspNet which uses a TSDF input, a voxel-based encoder, and a PointNet decoder for predicting grasp quality. Experiments with the other encoder/decoder architectures are provided in appendix C.

## 4 Experiments

### 4.1 Evaluation in Simulation

**Experimental setup.** For training and evaluation, we use the simulation benchmark from VGN [22], which has also been used in [31, 15]. While other grasping benchmarks exist, such as [40], they consist of fixed data that cannot be used to predict and test the grasping success from any view and in unseen areas of the scene, which is an important aspect of our method. In the VGN setup, simulated objects in Pybullet [41] are spawned in a random ‘pile’ or are ‘packed’ upright on a table. The benchmark consists of 343 objects split into 303 training and 40 testing objects. On average, five objects are spawned per scene. The only modification we do to make the task more realistic and challenging is to *randomize* the camera viewing angle when generating the scene TSDF or pointcloud.

**Data generation and training.** Unlike semi-implicit methods like VGN and GIGA [31], our network is fully implicit in the 6 grasp dimensions. Thus, we need a dataset with a larger number of grasps per scene to learn to discriminate grasps in SE(3). For this, we generate our grasp dataset using the sampling method of section 3.2 on the ground truth scenes. The candidate grasps are executed in simulation to get their labels (success/fail). We generate a dataset of 1.4 million grasps in 33,313 scenes for ‘pile’ scenes and 1.2 million grasps in 33,534 scenes for ‘packed’ scenes, balanced with both successful and unsuccessful grasps. We also sample 100,000 occupancy points per scene for training the scene reconstruction. A detailed description of the dataset generation is in appendix B.

**Baselines & metrics.** We compare our method against strong baselines in the literature that use different representations for predicting grasp quality. Due to the scope of our work, we compare mainly with methods that are implicit or semi-implicit. Particularly, we compare against the implicit methods **PointNetGPD** [14], a method that operates directly on pointclouds, and the current state-of-the-art **EdgeGraspNet** [15] that proposes a new contact-edge-based representation of grasps. Note that for **EdgeGraspNet\***, we generate the dataset according to the sampling strategy provided by [15] as it requires grasps samples on edges, but we use the same camera-view setup as ours. Therefore, this method uses the same dataset size but not the same labels of grasps, as it is not possible to directly use our dataset to train this method; hence it is marked with a \*.

Additionally, we compare with the semi-implicit methods **VGN** [22] and **GIGA** [31], with the latter considering scene reconstruction as an auxiliary loss. We train VGN and GIGA with high-resolution TSDFs (as also done for NeuGraspNet), as it leads to better performance. We also run ablations of our model with different settings, e.g., with and without scene rendering, etc., to demonstrate the efficacy of our full model. We train all methods from scratch on our dataset with random-view (random elevation between 15 and 75 degrees) pointcloud or TSDF inputs for a fair comparison. More details about the training setup and evaluation can be found in appendix B.

The main focus of this work is to evaluate the representation power and efficiency of NeuGraspNet, which learns the interaction between scene/object geometry and the robot end-effector for detecting high-quality 6DoF grasps. Our benchmarking setup consists, therefore, of three settings. (I) **Fixed Top View**: In this setting, the camera is placed at a fixed viewing angle: a 60-degree elevation, and at a distance of twice the workspace width (width in this setup is 30cm) – this setup is the one adopted by [31]. (II) **Random view**: This setup resembles the one of the training; the viewing angle is randomly chosen to be between 15 and 75-degree elevation, and the distance of the camera w.r.t. the scene ground plane is sampled between 1.6 to 2.4 times the workspace width. This setting is harder than the one used

Table 1: Ablation results of NeuGraspNet on Pile and Packed scenes

Pile scenes						
Method	Fixed Top View		Random View		Hard View	
	GSR (%)	DR (%)	GSR (%)	DR (%)	GSR (%)	DR (%)
NeuGraspNet	86.51 ± 1.42	83.52 ± 2.24	<b>85.05 ± 1.25</b>	<b>84.37 ± 1.52</b>	<b>73.95 ± 1.26</b>	<b>70.67 ± 1.69</b>
No-scene-render	85.79 ± 1.38	83.44 ± 2.40	83.57 ± 1.91	83.06 ± 1.50	69.71 ± 2.48	65.61 ± 3.37
No-local-render	79.83 ± 2.06	77.22 ± 2.72	77.04 ± 2.57	76.17 ± 2.51	63.51 ± 3.05	58.24 ± 3.14
No-local-occ	<b>86.62 ± 1.75</b>	<b>83.74 ± 2.41</b>	84.37 ± 1.51	83.72 ± 0.89	72.08 ± 1.47	69.10 ± 2.13
No rendering	73.59 ± 1.58	72.92 ± 2.82	73.36 ± 0.84	72.79 ± 1.38	56.52 ± 1.11	50.30 ± 2.75
Packed scenes						
Method	Fixed Top View		Random View		Hard View	
	GSR (%)	DR (%)	GSR (%)	DR (%)	GSR (%)	DR (%)
NeuGraspNet	<b>97.65 ± 0.92</b>	<b>93.16 ± 1.48</b>	<b>92.49 ± 1.41</b>	<b>91.74 ± 1.24</b>	<b>78.76 ± 1.89</b>	<b>82.80 ± 1.50</b>
No-scene-render	97.18 ± 1.14	92.80 ± 1.75	89.83 ± 1.79	90.19 ± 1.57	56.43 ± 4.62	29.08 ± 3.10
No-local-render	96.31 ± 0.93	92.17 ± 1.43	89.81 ± 1.37	90.10 ± 0.70	73.86 ± 3.31	76.12 ± 2.16
No-local-occ	96.53 ± 1.53	92.24 ± 1.37	90.62 ± 2.13	90.29 ± 1.56	78.14 ± 2.04	80.70 ± 1.73
No rendering	93.65 ± 0.76	91.46 ± 0.37	87.32 ± 1.89	88.34 ± 1.47	52.17 ± 4.12	26.88 ± 2.31

in [15] that considers angles between 30 and 45 degrees. (III) **Hard view**: While we sample the camera’s distance like the random view setting, we fix the viewing angle at 15 degrees. We argue that such views are realistic for robots like mobile manipulators that can move in the scene to grasp scattered objects with a limited field of view. Other methods that use fixed manipulators operating on tabletop surfaces have not considered such a setting. All these settings are tested on the ‘pile’ and ‘packed’ scenes of [22]. As metrics, we use the same metrics as [31, 22], namely, the Grasp Success Rate (GSR), i.e., the percentage of grasps that are successfully executed by the robot w.r.t. the total attempts per seen, and the Declutter Rate (DR), i.e., the percentage of objects removed successfully to the number of total objects presented in the scene. We perform 100 simulation rounds for 5 random seeds in all cases and report the average percentage and standard deviation per metric. As per the experiment setup of [22], one simulation round ends when (a) no objects remain, (b) no high-quality grasps are found, or (c) two consecutive failed grasp attempts have occurred.

**Ablation study.** Table 1 presents an ablation of different components of NeuGraspNet (full model at the top of the table) for evaluating and justifying the contribution of each component in the final network. As seen by the results, a model without any rendering (global or local), shown at the bottom of each sub-table, performs the worst, as in this case, the grasp sampler relies only on the pointcloud, and the grasp quality network struggles to discriminate in the SE(3) space. When we only remove the global scene-level surface rendering, we are able to achieve good performance both in fixed and random views evaluation settings, but we see a significant drop in performance for the hard view setting. This is understandable since, in those cases, a lot of the scene is unseen, hence, the grasp sampler struggles to sample reasonable candidate grasps. Removing the local render at the grasp level from NeuGraspNet significantly hurts performance, underlying the importance of the geometric features that allow learning the interaction of object surface and robotic gripper. Notably, we observe an equal or worse performance when removing the local occupancy supervision, especially when we observe the declutter rate in the ‘packed’ scenes, where the objects are placed very close to each other, and the scene occupancy may not provide fine details between the objects. In this case, providing a strong refinement signal for the local object occupancy improves performance. Additional ablations are provided in appendix C.

**Comparison with baselines.** Observing Table 2, we see that NeuGraspNet compares favorably against baselines in almost all experimental settings. In ‘pile’ scenes, which are more unstructured, NeuGraspNet has superior performance in all settings. Regarding the baselines, it is worth noting that EdgeGraspNet and GIGA perform similarly in GSR, but EdgeGraspNet has a higher DR, indicating that it exhibits fewer consecutive failures than GIGA. When looking at the ‘packed’ scenes, we observe a similar high performance by NeuGraspNet. However, there are interesting remarks regarding the baselines. GIGA performs very well in the fixed top view setting (that was key in [31]), thanks to the every-3d-voxel grasp sampling strategy. VGN, which shares the sampling strategy of GIGA, performs close to GIGA in random and hard views. PointNetGPD performs reasonably well in the fixed top view setting because it uses GPG as the grasp sampling strategy, which favors top grasps. However, it performs very poorly in the hard view setting since the top surfaces of the packed objects are rarely observed. EdgeGraspNet showcases a consistent behavior in ‘packed’ scenes. It also outperforms NeuGraspNet by  $\sim 2.5\%$  in GSR and DR in the hard view setting. Note that we

Table 2: Comparative results of NeuGraspNet and baselines on Pile and Packed scenes

Pile scenes						
Method	Fixed Top View		Random View		Hard View	
	GSR (%)	DR (%)	GSR (%)	DR (%)	GSR (%)	DR (%)
NeuGraspNet (ours)	<b>86.51 ± 1.42</b>	<b>83.52 ± 2.24</b>	<b>85.05 ± 1.25</b>	<b>84.37 ± 1.52</b>	<b>73.95 ± 1.26</b>	<b>70.67 ± 1.69</b>
PointNetGPD [14]	79.79 ± 2.28	77.81 ± 2.79	70.94 ± 3.12	68.88 ± 3.11	47.42 ± 3.40	36.02 ± 3.68
EdgeGraspNet* [15]	80.25 ± 1.41	83.18 ± 1.43	78.76 ± 1.16	80.89 ± 2.65	68.11 ± 2.63	69.32 ± 3.79
VGN [22]	77.44 ± 2.15	63.98 ± 5.03	78.48 ± 1.45	74.09 ± 1.16	68.46 ± 2.55	64.14 ± 4.37
GIGA [31]	82.92 ± 2.08	73.58 ± 2.93	78.67 ± 1.86	75.99 ± 1.79	69.13 ± 4.43	64.83 ± 5.63
Packed scenes						
Method	Fixed Top View		Random View		Hard View	
	GSR (%)	DR (%)	GSR (%)	DR (%)	GSR (%)	DR (%)
NeuGraspNet (ours)	<b>97.65 ± 0.92</b>	<b>93.16 ± 1.48</b>	<b>92.49 ± 1.41</b>	<b>91.74 ± 1.24</b>	78.76 ± 1.89	82.80 ± 1.50
PointNetGPD [14]	81.14 ± 2.52	86.04 ± 1.50	71.94 ± 1.38	76.23 ± 2.51	25.15 ± 2.61	14.18 ± 1.50
EdgeGraspNet* [15]	85.09 ± 2.48	85.36 ± 2.74	86.06 ± 0.75	86.51 ± 0.92	<b>81.61 ± 1.41</b>	<b>85.11 ± 0.84</b>
VGN [22]	83.42 ± 0.85	54.08 ± 5.35	78.11 ± 0.81	60.13 ± 1.96	70.27 ± 3.18	38.57 ± 3.40
GIGA [31]	96.05 ± 0.20	76.81 ± 3.21	87.99 ± 0.84	75.64 ± 2.75	73.87 ± 1.57	68.52 ± 4.49

train EdgeGraspNet on a different dataset (of equal size to ours), but with the grasp parameterization of [15] and test with their proposed edge grasp sampling strategy. In ‘packed’ scenes, this edge grasp detection strategy favors side grasps, unlike GPG, which favors top grasps. This characteristic of GPG also hurts the performance of NeuGraspNet in hard view settings. While we have shown increased gains by our enhanced scene-level GPG approach (cf. section 3.2), we note that a different geometrically-informed sampling strategy could lead to greater improvements. Nevertheless, we demonstrate that our local point and feature set successfully encodes the gripper-object complementarity and is a promising approach for future investigation.

## 4.2 Real-world evaluation

We perform a real-world experiment with a mobile manipulator robot TIAGo++ equipped with a head-mounted RGBD camera. The robot can place itself anywhere around a table with objects placed randomly in a ‘pile’ or ‘packed’ setting. We use 12 objects from the YCB dataset [42] for this experiment. For each setting, we perform 5 decluttering rounds and report the GSR and DR observed during real-world execution. Fig. 4 shows an example of the robot perceiving the scene from an arbitrary viewpoint and executing a grasp detected by NeuGraspNet. We observe a GSR and DR of 81.80 % and 76.92 %, respectively, for ‘pile’ scenes and a GSR and DR of 90.48 % and 92.59 %, respectively, for ‘packed’ scenes. We note that the drop in performance compared to section 4.1 is due to several factors. The execution of grasps on objects of relatively large width can sometimes fail due to imprecise perception or execution by the robot, hurting the GSR. On the other hand, very thin objects are not always clearly perceived by the depth camera since it is difficult to differentiate between the object and the table, hurting the DR. Nevertheless, with the use of better camera depth estimation techniques, we expect to get even better performance and enable effective real-world de-cluttering of scenes. Additional details and results are provided in appendix C and videos at: <https://sites.google.com/view/neugraspnet>.

## 4.3 Limitations

As noted earlier, one limitation of our work is in the use of the inductive bias induced by the GPG sampler. While we have improved it with our approach (cf. section 3.2) we can still observe difficulties in sampling meaningful grasps in SE(3). Future research involves investigating and learning sampling strategies on a manifold diffeomorphic to SE(3) (or SO(3)) or considering symmetries to enhance the grasp proposal generation. An additional caveat of NeuGraspNet is the computational overhead of the multiple surface rendering processes, which leads to an average overhead in inference time of about 5.5 sec. Nevertheless, we posit that advances in neural rendering [43] can make such methods increasingly accessible even with onboard computing. A further limitation that transcends our method, and affects most grasp detection approaches, is that grasp execution is done in an open-loop fashion; once a high-quality grasp is detected, execution is done via planning methods that do not get feedback about sudden changes in the scene. Thus, coupling grasp detection (perception) and manipulation (action) is part of our plans. Finally, all described methods’



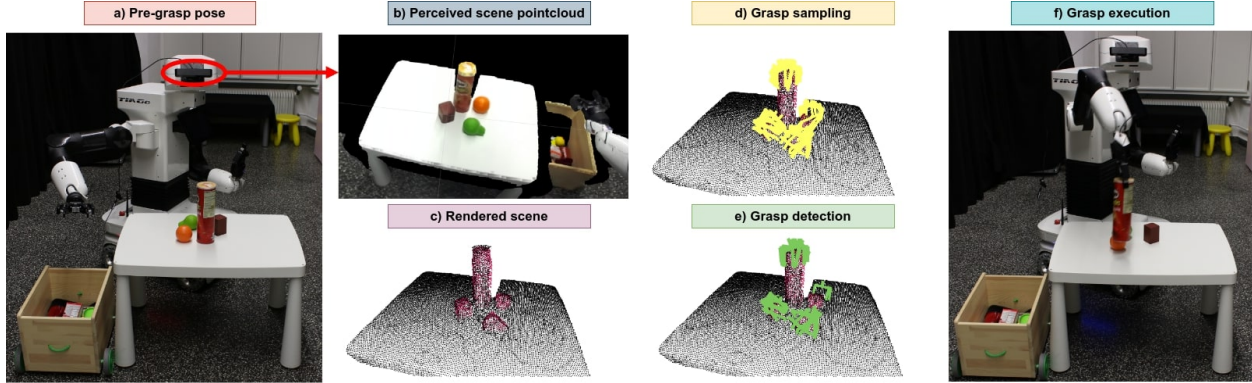


Figure 4: Real-world evaluation of NeuGraspNet with a mobile manipulator robot. The robot starts from a pre-grasp pose (a), and perceives the scene pointcloud (b). NeuGraspNet renders and completes the scene (c), runs 6DoF grasp sampling (d), and detects high-quality grasps (e). The robot executes grasps with classical motion planning, dropping collected objects in the box (f).

limitations stem from relying only on 3D perception. We postulate that enhancing grasp detection with additional textural or semantic information would allow better scene understanding and consequent grasp selection and execution.

## 5 Conclusion and Broader Impact

We presented NeuGraspNet, a novel full implicit 6DoF-grasp prediction method that re-imagines robotic grasping as surface rendering. NeuGraspNet can predict high-fidelity grasps from any random viewpoint of a scene populated with objects without requiring additional scene exploration. Our method learns an implicit geometric representation of the scene and uses the learned geometry to perform global rendering to sample grasps even in unseen parts of the workspace. Treating the robotic gripper as a multi-camera system, we also render and supervise the relevant surface of objects to extract local information and features that allow learning grasp quality in the challenging  $SE(3)$  space. We demonstrated the superior performance of NeuGraspNet in simulated experiments of varying difficulty, showcasing superior performance against various baselines in the literature. Finally, we manifested the real-world applicability of NeuGraspNet in mobile robotic grasping experiments.

Robotics greatly needs high-fidelity 3D geometric reasoning that would positively impact various sectors. Our method leverages neural representation learning to extract the 3D geometry of scenes to allow robots to interact with objects in the real world. However, possible misinterpretation of the scene due to the supervised learning objectives could lead to grasping errors that could damage objects or the robot. Thus, we encourage the deployment of this research with additional safeguards. Nevertheless, we foresee great societal benefits by empowering robots with 3D spatial reasoning.

## Acknowledgements

This work was supported by the German Research Foundation (DFG) Emmy Noether Programme (#448644653). We also gratefully acknowledge the computing time provided to us on the high-performance computer Lichtenberg at the NHR Centers NHR4CES at TU Darmstadt, Germany. This is funded by the Federal Ministry of Education and Research, and the state governments participating on the basis of the resolutions of the GWK for national high-performance computing at universities ([www.nhr-verein.de/unsere-partner](http://www.nhr-verein.de/unsere-partner)).

## References

- [1] Jeffrey Mahler, Jacky Liang, Sherdil Niyaz, Michael Laskey, Richard Doan, Xinyu Liu, Juan Aparicio Ojea, and Ken Goldberg. Dex-net 2.0: Deep learning to plan robust grasps with synthetic point clouds and analytic grasp metrics. *arXiv preprint arXiv:1703.09312*, 2017.
- [2] Jeffrey Mahler, Matthew Matl, Xinyu Liu, Albert Li, David Gealy, and Ken Goldberg. Dex-net 3.0: Computing robust vacuum suction grasp targets in point clouds using a new analytic model and deep learning. In *2018 IEEE International Conference on robotics and automation (ICRA)*, pages 5620–5627. IEEE, 2018.
- [3] Douglas Morrison, Peter Corke, and Jürgen Leitner. Learning robust, real-time, reactive robotic grasping. *The International journal of robotics research*, 39(2-3):183–201, 2020.
- [4] Georgia Chalvatzaki, Nikolaos Gkanatsios, Petros Maragos, and Jan Peters. Orientation attentive robotic grasp synthesis with augmented grasp map representation. *arXiv preprint arXiv:2006.05123*, 2020.
- [5] Oliver Kroemer, Scott Niekum, and George Konidaris. A review of robot learning for manipulation: Challenges, representations, and algorithms. *The Journal of Machine Learning Research*, 22(1):1395–1476, 2021.
- [6] Rhys Newbury, Morris Gu, Lachlan Chumbley, Arsalan Mousavian, Clemens Eppner, Jürgen Leitner, Jeannette Bohg, Antonio Morales, Tamim Asfour, Danica Kragic, et al. Deep learning approaches to grasp synthesis: A review. *arXiv preprint arXiv:2207.02556*, 2022.
- [7] Snehal Jauhri, Jan Peters, and Georgia Chalvatzaki. Robot learning of mobile manipulation with reachability behavior priors. *IEEE Robotics and Automation Letters*, 7(3):8399–8406, 2022.
- [8] Jiaheng Hu, Peter Stone, and Roberto Martín-Martín. Causal policy gradient for whole-body mobile manipulation. *arXiv preprint arXiv:2305.04866*, 2023.
- [9] Arsalan Mousavian, Clemens Eppner, and Dieter Fox. 6-dof graspnet: Variational grasp generation for object manipulation. In *ICCV*, pages 2901–2910. IEEE, 2019.
- [10] Minghao Gou, Hao-Shu Fang, Zhanda Zhu, Sheng Xu, Chenxi Wang, and Cewu Lu. Rgb matters: Learning 7-dof grasp poses on monocular rgbd images. In *2021 IEEE International Conference on Robotics and Automation (ICRA)*, pages 13459–13466. IEEE, 2021.
- [11] Chenxi Wang, Hao-Shu Fang, Minghao Gou, Hongjie Fang, Jin Gao, and Cewu Lu. Graspness discovery in clutters for fast and accurate grasp detection. In *Proceedings of the IEEE/CVF International Conference on Computer Vision*, pages 15964–15973, 2021.
- [12] Martin Sundermeyer, Arsalan Mousavian, Rudolph Triebel, and Dieter Fox. Contact-graspnet: Efficient 6-dof grasp generation in cluttered scenes. In *ICRA*, pages 13438–13444. IEEE, 2021.
- [13] Andreas ten Pas, Marcus Gualtieri, Kate Saenko, and Robert Platt Jr. Grasp pose detection in point clouds. *Int. J. Robotics Res.*, 36(13-14):1455–1473, 2017.
- [14] Hongzhuo Liang, Xiaojian Ma, Shuang Li, Michael Görner, Song Tang, Bin Fang, Fuchun Sun, and Jianwei Zhang. Pointnetgpd: Detecting grasp configurations from point sets. In *ICRA*, pages 3629–3635. IEEE, 2019.
- [15] Haojie Huang, Dian Wang, Xupeng Zhu, Robin Walters, and Robert Platt. Edge grasp network: A graph-based se(3)-invariant approach to grasp detection. *ICRA*, 2023.
- [16] Jianglong Ye, Jiashun Wang, Binghao Huang, Yuzhe Qin, and Xiaolong Wang. Learning continuous grasping function with a dexterous hand from human demonstrations. *IEEE Robotics and Automation Letters*, 8(5): 2882–2889, 2023. doi: 10.1109/LRA.2023.3261745.
- [17] Sammy Christen, Muhammed Kocabas, Emre Aksan, Jemin Hwangbo, Jie Song, and Otmar Hilliges. D-grasp: Physically plausible dynamic grasp synthesis for hand-object interactions. In *Proceedings of the IEEE/CVF Conference on Computer Vision and Pattern Recognition (CVPR)*, pages 20577–20586, June 2022.
- [18] Haoming Li, Xinzhuo Lin, Yang Zhou, Xiang Li, Yuchi Huo, Jiming Chen, and Qi Ye. Contact2grasp: 3d grasp synthesis via hand-object contact constraint, 2023.
- [19] Thomas Weng, David Held, Franziska Meier, and Mustafa Mukadam. Neural grasp distance fields for robot manipulation. *arXiv preprint arXiv:2211.02647*, 2022.
- [20] Julen Urain, Niklas Funk, Georgia Chalvatzaki, and Jan Peters. Se(3)-diffusionfields: Learning cost functions for joint grasp and motion optimization through diffusion. *arXiv preprint arXiv:2209.03855*, 2022.
- [21] Peiyuan Ni, Wenguang Zhang, Xiaoxiao Zhu, and Qixin Cao. Pointnet++ grasping: Learning an end-to-end spatial grasp generation algorithm from sparse point clouds. In *2020 IEEE International Conference on Robotics and Automation (ICRA)*, pages 3619–3625. IEEE, 2020.

- [22] Michel Breyer, Jen Jen Chung, Lionel Ott, Roland Siegwart, and Juan I. Nieto. Volumetric grasping network: Real-time 6 DOF grasp detection in clutter. In *CoRL*, volume 155 of *Proceedings of Machine Learning Research*, pages 1602–1611. PMLR, 2020.
- [23] Kuang-Yu Jeng, Yueh-Cheng Liu, Zhe Yu Liu, Jen-Wei Wang, Ya-Liang Chang, Hung-Ting Su, and Winston Hsu. Gdn: A coarse-to-fine (c2f) representation for end-to-end 6-dof grasp detection. In *Conference on Robot Learning*, pages 220–231. PMLR, 2021.
- [24] Hao-Shu Fang, Chenxi Wang, Hongjie Fang, Minghao Gou, Jirong Liu, Hengxu Yan, Wenhai Liu, Yichen Xie, and Cewu Lu. Anygrasp: Robust and efficient grasp perception in spatial and temporal domains. *arXiv preprint arXiv:2212.08333*, 2022.
- [25] Lars M. Mescheder, Michael Oechsle, Michael Niemeyer, Sebastian Nowozin, and Andreas Geiger. Occupancy networks: Learning 3d reconstruction in function space. In *CVPR*, pages 4460–4470. Computer Vision Foundation / IEEE, 2019.
- [26] Songyou Peng, Michael Niemeyer, Lars M. Mescheder, Marc Pollefeys, and Andreas Geiger. Convolutional occupancy networks. In *ECCV*, volume 12348, pages 523–540, 2020.
- [27] Jeong Joon Park, Peter Florence, Julian Straub, Richard A. Newcombe, and Steven Lovegrove. DeepSDF: Learning continuous signed distance functions for shape representation. In *CVPR*, pages 165–174. Computer Vision Foundation / IEEE, 2019.
- [28] Peng Wang, Lingjie Liu, Yuan Liu, Christian Theobalt, Taku Komura, and Wenping Wang. Neus: Learning neural implicit surfaces by volume rendering for multi-view reconstruction. In *NeurIPS*, pages 27171–27183, 2021.
- [29] Michael Oechsle, Songyou Peng, and Andreas Geiger. UNISURF: unifying neural implicit surfaces and radiance fields for multi-view reconstruction. In *ICCV*, pages 5569–5579. IEEE, 2021.
- [30] Lior Yariv, Jiatao Gu, Yoni Kasten, and Yaron Lipman. Volume rendering of neural implicit surfaces. *Advances in Neural Information Processing Systems*, 34:4805–4815, 2021.
- [31] Zhenyu Jiang, Yifeng Zhu, Maxwell Svetlik, Kuan Fang, and Yuke Zhu. Synergies between affordance and geometry: 6-dof grasp detection via implicit representations. In *Robotics: Science and Systems*, 2021.
- [32] Qiyu Dai, Yan Zhu, Yiran Geng, Ciyu Ruan, Jiazhao Zhang, and He Wang. Graspnerf: Multiview-based 6-dof grasp detection for transparent and specular objects using generalizable nerf. *arXiv preprint arXiv:2210.06575*, 2022.
- [33] Jens Lundell, Francesco Verdoja, and Ville Kyrki. Ddgc: Generative deep dexterous grasping in clutter. *IEEE Robotics and Automation Letters*, 6(4):6899–6906, 2021. doi: 10.1109/LRA.2021.3096239.
- [34] Michael Niemeyer, Lars Mescheder, Michael Oechsle, and Andreas Geiger. Differentiable volumetric rendering: Learning implicit 3d representations without 3d supervision. In *Proceedings of the IEEE/CVF Conference on Computer Vision and Pattern Recognition*, pages 3504–3515, 2020.
- [35] Ben Mildenhall, Pratul P. Srinivasan, Matthew Tancik, Jonathan T. Barron, Ravi Ramamoorthi, and Ren Ng. Nerf: Representing scenes as neural radiance fields for view synthesis. In *ECCV*, volume 12346, pages 405–421, 2020.
- [36] Marcus Gualtieri, Andreas ten Pas, Kate Saenko, and Robert Platt Jr. High precision grasp pose detection in dense clutter. In *IROS*, pages 598–605. IEEE, 2016.
- [37] Congyue Deng, Or Litany, Yueqi Duan, Adrien Poulénard, Andrea Tagliasacchi, and Leonidas J. Guibas. Vector neurons: A general framework for so(3)-equivariant networks. In *ICCV*, pages 12180–12189. IEEE, 2021.
- [38] Charles Ruizhongtai Qi, Hao Su, Kaichun Mo, and Leonidas J. Guibas. Pointnet: Deep learning on point sets for 3d classification and segmentation. In *CVPR*, pages 77–85. IEEE Computer Society, 2017.
- [39] Yue Wang, Yongbin Sun, Ziwei Liu, Sanjay E. Sarma, Michael M. Bronstein, and Justin M. Solomon. Dynamic graph CNN for learning on point clouds. *ACM Trans. Graph.*, 38(5):146:1–146:12, 2019.
- [40] Hao-Shu Fang, Chenxi Wang, Minghao Gou, and Cewu Lu. Graspnet-1billion: A large-scale benchmark for general object grasping. In *Proceedings of the IEEE/CVF conference on computer vision and pattern recognition*, pages 11444–11453, 2020.
- [41] Erwin Coumans and Yunfei Bai. Pybullet, a python module for physics simulation for games, robotics and machine learning. <http://pybullet.org>, 2016–2021.
- [42] Berk Calli, Aaron Walsman, Arjun Singh, Siddhartha Srinivasa, Pieter Abbeel, and Aaron M Dollar. Benchmarking in manipulation research: The ycb object and model set and benchmarking protocols. *arXiv preprint arXiv:1502.03143*, 2015.

- [43] Thomas Müller, Alex Evans, Christoph Schied, and Alexander Keller. Instant neural graphics primitives with a multiresolution hash encoding. *ACM Trans. Graph.*, 41(4):102:1–102:15, July 2022. doi: 10.1145/3528223.3530127. URL <https://doi.org/10.1145/3528223.3530127>.
- [44] Alexandre Boulch and Renaud Marlet. Poco: Point convolution for surface reconstruction. In *Proceedings of the IEEE/CVF Conference on Computer Vision and Pattern Recognition*, pages 6302–6314, 2022.
- [45] Yunlu Chen, Basura Fernando, Hakan Bilen, Matthias Nießner, and Efstratios Gavves. 3d equivariant graph implicit functions. In *ECCV 2022: 17th European Conference, Tel Aviv, Israel, October 23–27, 2022, Proceedings, Part III*, pages 485–502. Springer, 2022.
- [46] Zhen Wang, Shijie Zhou, Jeong Joon Park, Despoina Paschalidou, Suya You, Gordon Wetzstein, Leonidas Guibas, and Achuta Kadambi. Alto: Alternating latent topologies for implicit 3d reconstruction. *CVPR*, 2023.
- [47] Karun B Shimoga. Robot grasp synthesis algorithms: A survey. *The International Journal of Robotics Research*, 15(3):230–266, 1996.
- [48] Jeannette Bohg, Antonio Morales, Tamim Asfour, and Danica Kragic. Data-driven grasp synthesis—a survey. *IEEE Transactions on robotics*, 30(2):289–309, 2013.
- [49] Jens Lundell, Francesco Verdoja, Tran Nguyen Le, Arsalan Mousavian, Dieter Fox, and Ville Kyrki. Constrained generative sampling of 6-dof grasps. *arXiv preprint arXiv:2302.10745*, 2023.
- [50] Antonio Alliegro, Martin Rudorfer, Fabio Frattin, Aleš Leonardis, and Tatiana Tommasi. End-to-end learning to grasp via sampling from object point clouds. *IEEE Robotics and Automation Letters*, 7(4):9865–9872, 2022.
- [51] Chaozheng Wu, Jian Chen, Qiaoyu Cao, Jianchi Zhang, Yunxin Tai, Lin Sun, and Kui Jia. Grasp proposal networks: An end-to-end solution for visual learning of robotic grasps. *Advances in Neural Information Processing Systems*, 33:13174–13184, 2020.
- [52] Seyed S Mohammadi, Nuno F Duarte, Dimitris Dimou, Yiming Wang, Matteo Taiana, Pietro Morerio, Atabak Dehban, Plinio Moreno, Alexandre Bernardino, Alessio Del Bue, et al. 3dsgrasp: 3d shape-completion for robotic grasp. *arXiv preprint arXiv:2301.00866*, 2023.
- [53] Lirui Wang, Xiangyun Meng, Yu Xiang, and Dieter Fox. Hierarchical policies for cluttered-scene grasping with latent plans. *IEEE Robotics and Automation Letters*, 7(2):2883–2890, 2022.
- [54] Yiye Chen, Ruinian Xu, Yunzhi Lin, and Patricio A Vela. Kgnv2: Separating scale and pose prediction for keypoint-based 6-dof grasp pose synthesis on rgb-d input. *arXiv preprint arXiv:2303.05617*, 2023.
- [55] Yiye Chen, Yunzhi Lin, and Patricio Vela. Keypoint-graspnet: Keypoint-based 6-dof grasp generation from the monocular rgb-d input. *arXiv preprint arXiv:2209.08752*, 2022.
- [56] Junhao Cai, Jun Cen, Haokun Wang, and Michael Yu Wang. Real-time collision-free grasp pose detection with geometry-aware refinement using high-resolution volume. *IEEE Robotics and Automation Letters*, 7(2):1888–1895, 2022.
- [57] Xinchun Yan, Jasmined Hsu, Mohammad Khansari, Yunfei Bai, Arkanath Pathak, Abhinav Gupta, James Davidson, and Honglak Lee. Learning 6-DoF grasping interaction via deep geometry-aware 3d representations. In *IEEE International Conference on Robotics and Automation*, 2018.
- [58] Zhixuan Liu, Zibo Chen, Shangjin Xie, and Wei-Shi Zheng. Transgrasp: A multi-scale hierarchical point transformer for 7-dof grasp detection. In *2022 International Conference on Robotics and Automation (ICRA)*, pages 1533–1539. IEEE, 2022.
- [59] Dinh-Cuong Hoang, Johannes A Stork, and Todor Stoyanov. Context-aware grasp generation in cluttered scenes. In *2022 International Conference on Robotics and Automation (ICRA)*, pages 1492–1498. IEEE, 2022.
- [60] Charles R Qi, Or Litany, Kaiming He, and Leonidas J Guibas. Deep hough voting for 3d object detection in point clouds. In *proceedings of the IEEE/CVF International Conference on Computer Vision*, pages 9277–9286, 2019.
- [61] Junhao Cai, Jingcheng Su, Zida Zhou, Hui Cheng, Qifeng Chen, and Michael Y Wang. Volumetric-based contact point detection for 7-dof grasping. In *6th Annual Conference on Robot Learning*, 2022.
- [62] Ahmed H Qureshi, Arsalan Mousavian, Chris Paxton, Michael C Yip, and Dieter Fox. Nerp: Neural rearrangement planning for unknown objects. *arXiv preprint arXiv:2106.01352*, 2021.
- [63] Ninad Khargonkar, Neil Song, Zesheng Xu, Balakrishnan Prabhakaran, and Yu Xiang. Neuralgrasps: Learning implicit representations for grasps of multiple robotic hands. In *Conference on Robot Learning*, pages 516–526. PMLR, 2023.
- [64] Jeffrey Ichnowski, Yahav Avigal, Justin Kerr, and Ken Goldberg. Dex-nerf: Using a neural radiance field to grasp transparent objects. In *Conference on Robot Learning*, pages 526–536. PMLR, 2022.

# Appendices

## A Network architecture and implementation details

### A.1 Network architecture

The input to our network is a pointcloud or Truncated Signed Distance Field (TSDF) captured from a single viewpoint. We use an encoder-decoder architecture with scene reconstruction and grasp quality prediction heads. We predict grasp quality based on the features of the surface pointset that the grasp interacts with. For this, we use a feature point network decoder to classify successful/unsuccessful grasps. Using a common feature space for both scene reconstruction and grasp quality helps exploit synergies between these objectives [31]. The overall pipeline can be seen in fig. 1; our code is provided as part of the supplementary materials and will also be open-sourced upon acceptance.

#### A.1.1 Encoder

We use a similar encoder architecture as Convolutional Occupancy Networks (ConvONets) [26]. If the input is a scene voxel grid (eg. TSDF), ConvONets use a simple 3D encoder with ResNets and U-Nets. On the other hand, if a pointcloud input is provided, a ‘local’ PointNet is first used to encode the scene before the U-Net stage. We experiment with both versions of the encoder and report results in appendix C. The encoded 3D scene is represented using three 64x64 feature planes (one for each axis pair  $xy$ ,  $yz$ ,  $xz$ ). While many implicit networks have been proposed recently ([44, 45]), the ConvONet has some nice properties. Firstly, most other implicit reconstruction networks assume access to a full pointcloud of the scene, obtained by either sampling points on a mesh or using full 3D scans of scenes. The ConvONet, on the other hand, can reconstruct unseen parts of the scene by using a U-Net architecture over explicit feature grids/planes in the whole scene. Another advantage compared to other networks that utilize feature grids/planes [46] is the faster inference time of a ConvONet, which is essential in our case since we need to perform surface rendering on both the scene-level and grasp-level in real-robot scenarios.

**SE(3) Equivariance** Many recently proposed methods leverage  $SO(3)$  or  $SE(3)$  equivariance to make their networks more robust to rotations and translations [37, 15]. Since rotational equivariance could be a viable method of obtaining viewpoint-equivariant feature extraction in our approach, we also run experiments with an  $SO(3)$  equivariant encoder leveraging VectorNeurons [37]. Note that  $SO(3)$  equivariance cannot work on voxel or feature grids since they do not belong to the rotation group. However, we still want the local feature and scene completion capabilities of ConvONets. To solve this problem, we propose a hybrid VecNeuron-FeatureGrid encoder. The encoder uses a pointcloud input and encodes point-wise 3D equivariant features using a VectorNeuron architecture. These point-wise features are then pooled to obtain  $SO(3)$  *invariant* features that can then be projected into the feature planes of ConvONets. Experimental results from this encoder are reported in appendix C.

#### A.1.2 Decoder

The grasp decoder classifies each grasp as successful or unsuccessful, hence predicting grasp quality. For each grasp query, the surface rendering procedure gives us 3D points relevant to the grasp, while the encoded 3D representation provides features corresponding to these points. We transform the 3D surface points (fig. 3(b)) to the grasp (gripper) frame and concatenate them to the features. We also concatenate the grasp (gripper) position and orientation to these features. To finally predict the grasp quality, we use a feature point network to process this 3D feature pointcloud. We use two popular network architectures: PointNet [38] and DGCNN [39], comparative results of which are provided in appendix C. For scene reconstruction, we use the same ResNet-based decoder architecture as ConvONets.

Table 3: List of key network parameters used by *NeuGraspNet*

parameter	value	parameter	value	parameter	value	parameter	value
voxel resolution	64	latent dims	128	quality decoder points	1024	occupancy loss weight	2.0
plane resolution	64	hidden dims	256	quality decoder network	PointNet classic [38]	quality loss weight	1.0
U-Net depth	5	concat plane feats	True	occupancy decoder ResNets	5	local occ loss weight	1.0



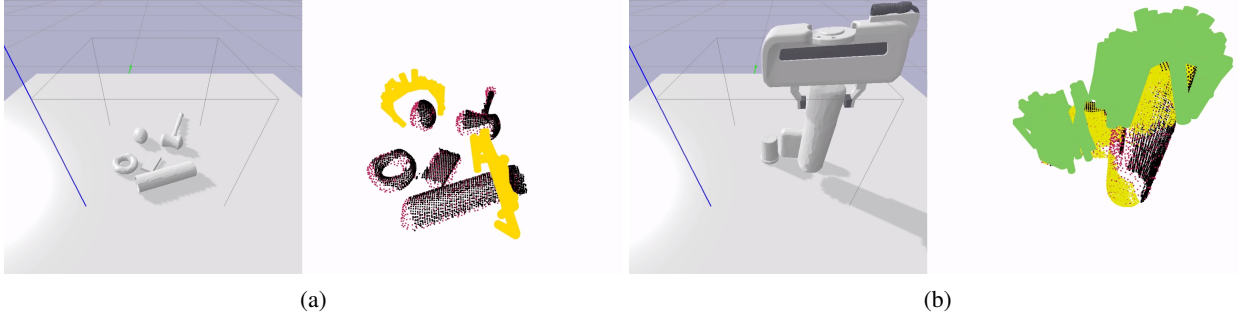


Figure 5: Simulated experiments with (a) pile and (b) packed scenes from the VGN [22] simulation benchmark. We also visualize our input scene pointcloud (black), our reconstructed pointcloud (red), candidate grasps (yellow), and high-quality grasps (green) executed by the gripper.

## B Additional details about experimental setup

### B.1 Dataset generation and training

Unlike semi-implicit methods like [22, 31], our network is fully implicit in 6 grasp dimensions, which requires a larger number of grasps per scene to learn to discriminate them in  $SE(3)$ . We use a similar procedure to generate grasps as in [22, 31]. We use the scene pointcloud sampled from ground-truth meshes from 33000 simulated scenes from the VGN setup. The pointclouds are cropped to within the 30 cm cube considered for grasping and fed to a GPG sampler [36]. We sample a maximum of 60 grasps per scene with a maximum budget of 240 points sampled by GPG. For occupancy prediction, we sample 100,000 points and their occupancies using uniform sampling in the scene volume.

As detailed in section 3.3, we also use local supervision for both grasp quality and scene reconstruction. We use the ground truth renderer in simulation to render the local surface points relevant for every grasp in our dataset. As shown in fig. 3(a), we use three cameras per grasp (one for every link of the gripper) placed 2.5 cm away from the link and render 64x64 depth images with a 120-degree field of view (FOV). We merge the surface pointclouds from the three cameras to generate our local grasp pointcloud. We filter out points outside the gripper by more than 1cm. We use a maximum of 1024 points per grasp and discard grasps with less than 50 points in their local surface cloud. We also add noise (gamma noise as in [31]) to these surface points and store the occupancy values of the points (fig. 3(c)). Training the grasp quality using these noisy pointclouds helps regularize against imperfect neural rendering at test time. Training the scene reconstruction with the occupancies of these noisy pointclouds helps precisely reconstruct regions close to the surfaces. We provide our data generation pipeline as part of our codebase.

We train all our networks on single NVIDIA V100 GPUs on which each training run takes about 36 hours to converge. We use 5% of the data for validation. In practice, learning rates between  $1e-4$  and  $5e-5$  work best for all the networks with a batch size of 32 data samples.

### B.2 Neural rendering

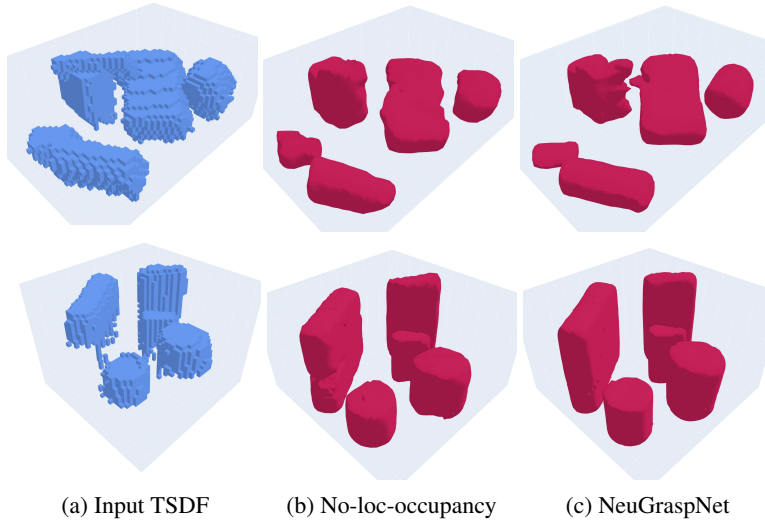
For the neural rendering of the implicit geometry at inference time, we use a two-stage depth prediction method as used in [34, 29]. The first stage proposes points along each ray originating from the camera and checks their occupancy using the occupancy network. The first point along a ray for which the occupancy changes from free space to occupied space is a rough estimation of the surface point. The second stage uses a secant search root-finding method along the smaller ray segment around the roughly estimated surface point. This search gives us the precise surface point.

For scene-level neural rendering, we use six cameras placed at a 60-degree elevation around the scene (fig. 2(b)). Each camera renders 64x64 images with a 90-degree FOV. We propose 256 proposal points along each ray at a maximum distance of  $3 \times (\text{size of the scene}) = 90$  cm, giving us a resolution of 0.0035 m. We then perform 8 secant search steps to refine the surface point estimation further.

For local grasp-level neural rendering, we use the same camera placement and settings used for the local supervision ground-truth rendering (64x64 images and 120-degree FOV). We propose 15 proposal points along each ray at a maximum distance of  $2 \times (\text{gripper width}) = 9$  cm. This gives us a resolution of 0.006 m. We then perform 8 secant search steps to further refine the surface point estimation to arrive at the rendered surface cloud visualized in fig. 3(b).

Table 4: Comparative results when using different encoder and decoder architectures

Method	Pile scenes					
	Fixed Top View		Random View		Hard View	
	GSR (%)	DR (%)	GSR (%)	DR (%)	GSR (%)	DR (%)
NeuGraspNet (3D Enc+PointNet Dec)	<b>86.51 ± 1.42</b>	<b>83.52 ± 2.24</b>	<b>85.05 ± 1.25</b>	<b>84.37 ± 1.52</b>	<b>73.95 ± 1.26</b>	<b>70.67 ± 1.69</b>
PointNet Encoder	79.26 ± 3.36	78.98 ± 2.61	77.82 ± 1.60	78.45 ± 2.72	66.64 ± 1.85	64.50 ± 1.82
VectorNeuron Encoder	79.21 ± 1.87	77.82 ± 2.92	77.28 ± 1.32	77.60 ± 1.88	63.57 ± 2.40	60.05 ± 3.30
DGCNN Decoder	84.91 ± 1.03	83.14 ± 1.54	81.80 ± 1.98	80.68 ± 2.14	68.63 ± 1.46	65.29 ± 2.45
Method	Packed scenes					
	Fixed Top View		Random View		Hard View	
	GSR (%)	DR (%)	GSR (%)	DR (%)	GSR (%)	DR (%)
NeuGraspNet (3D Enc+PointNet Dec)	<b>97.65 ± 0.92</b>	<b>93.16 ± 1.48</b>	<b>92.49 ± 1.41</b>	<b>91.74 ± 1.24</b>	<b>78.76 ± 1.89</b>	<b>82.80 ± 1.50</b>
PointNet Encoder	95.15 ± 1.86	90.40 ± 0.88	89.80 ± 1.94	88.97 ± 2.04	73.86 ± 1.64	77.15 ± 2.16
VectorNeuron Encoder	94.75 ± 0.63	90.61 ± 1.45	89.16 ± 2.77	89.10 ± 1.86	77.29 ± 2.84	80.05 ± 2.87
DGCNN Decoder	95.61 ± 0.73	93.01 ± 1.95	90.62 ± 1.83	90.78 ± 1.32	74.69 ± 2.58	79.94 ± 2.41

Figure 6: Example scene reconstructions in a ‘pile’ (top) and a ‘packed’ (bottom) scene. Networks trained *with* local occupancy supervision (c) are able to finely reconstruct the local surface.

## C Additional experimental results

### C.1 Additional comparisons/ablations

In table 4, we compare the results of NeuGraspNet against other encoder and decoder architectures as mentioned in appendix A. Notably, the network performance drops when an input pointcloud is used instead of the TSDF grid and the 3D Encoder. Thus, both the PointNet and our adapted VectorNeuron encoder versions of the network perform worse. In pile scenes, the VectorNeuron encoder does not provide any notable benefits but for packed scenes, we see that the VectorNeuron version performs better than the PointNet encoder with hard viewpoints. In the case of the grasp quality decoder, the DGCNN point decoder performs slightly worse than the PointNet decoder used in the final NeuGraspNet model. A possible explanation is that the DGCNN network could struggle to fit the data when the previously encoded latent features of the pointset change during training as the occupancy predictions change. These feature changes could cause issues in the dynamic knn feature graph generation performed by DGCNN.

### C.2 Scene reconstruction

We report the scene reconstruction results of NeuGraspNet qualitatively in fig. 6 and quantitatively in table 5. Though scene reconstruction is not the primary goal of our work, we run experiments to note how accurate the scene reconstruction needs to be to achieve the grasping results of NeuGraspNet. Moreover, we check the effect of our local occupancy supervision in ‘pile’ and ‘packed’ scenes. We reconstruct the scene mesh by querying the network over the volume

Table 5: Scene reconstruction results

Pile scenes		Packed scenes	
Method	IoU (%)	Method	IoU (%)
NeuGraspNet	73.22	NeuGraspNet	89.39
NeuGraspNet (No-local-occ)	73.48	NeuGraspNet (No-local-occ)	87.16

using the Multiresolution IsoSurface Extraction (MISE) method from [25]. We report the Intersection over Union (IoU) between the ground truth mesh and the reconstructed mesh in table 5. Notably, even though we use TSDF grids from randomized viewpoints in our problem setup (making reconstruction much more challenging than in [31]), the network still performs well. Consistent with the grasping results, local occupancy supervision is beneficial in ‘packed’ scenes leading to a higher IoU, but has a smaller effect in ‘pile’ scenes (table 5).

### C.3 Real-world experiments

To demonstrate the applicability of our method in the real-world, we perform grasping experiments with a TIAGo++ mobile manipulator with an omnidirectional base. We randomize the views of the scene by moving the robot’s base to the left or right of the table with a random orientation, moving the robot’s torso up or down, and moving the robot’s head toward the scene, as visualized in fig. 7(b). We use the same grasp sampling (GPG) and rendering settings as in simulations. Unlike the simulations, we use a Robotiq 2F-85 adaptive gripper for grasping. Thus, we generate another dataset from simulation using our dataset generation strategy with the Robotiq gripper. For depth estimation, we use a ZED2 Stereo Camera mounted over the head of the robot. To ensure sim-to-real transfer, we add more noise to the simulated depth cameras at the scene and grasp rendering levels. We use the MoveIt planning library to plan the robot arm’s movements. As grasp objects, we use objects from the YCB dataset [42] as visualized in fig. 7(a). We perform 5 trials each with ‘pile’ and ‘packed’ scenes for the random-view setting and report a GSR and DR of **81.80 %** and **76.92 %**, respectively, for ‘pile’ scenes and a GSR and DR of **90.48 %** and **92.59 %**, respectively, for ‘packed’ scenes. Video demonstrations of the real-world grasp execution are provided in the supplementary material and are also available at <https://sites.google.com/view/neugraspnet>. Notably, we still place the robot close to the table to ensure that most of the predicted grasps are *reachable*. However, in many real-world cases, this may not be the case since the robot could be placed anywhere in a scene. In future work, we aim to address this limitation by incorporating a reachability metric into the grasp quality.

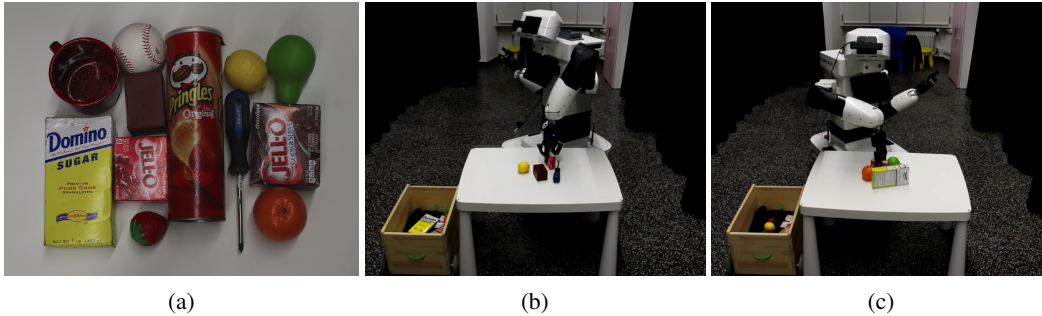


Figure 7: Real-world experiments. We use a subset of the YCB [42] objects (a) for the grasping experiments. To make the setup more realistic we move the mobile manipulator and randomize the views (Eg. (b) and (c)) after every grasp execution.

## D Related Work

Robotic grasping has been studied analytically and with data-driven models [47, 48]. Yet remains a vastly unsolved problem, especially when it comes to 6DoF grasping in open, cluttered scenes that go beyond table-top grasping. A comprehensive review on deep grasp synthesis is introduced in [6]. We refer, here, to a subset of works covering some explicit grasp generative models and implicit (discriminative models) and semi-implicit methods

**Explicit grasp generation.** Sampling efficient grasps, especially in partially-observed objects, greatly hinders grasp prediction [49–51]. GraspNet [9] is a variational autoencoder generative model that learns a grasp distribution in  $SE(3)$  but additionally relies on an iterative refinement process. [52] proposes using scene completion to sample grasps. A hierarchical end-to-end learning approach for generating collision-free grasps in cluttered scenes is proposed in [53]. In [10, 11] the authors demonstrated the complementarity between RGB and pointcloud data for learning to generate grasp poses while predicting graspness over piled scenes. AnyGrasp [24] is a spatiotemporal approach for finding temporal associations among grasps across every two observations. ContactGraspNet[12] motivates a reduced grasp representation on the fact at least one of two contact points of the gripper is visible in a pointcloud prior to grasping, therefore proposes a grasp parametrization w.r.t. the contact point assumption, leading to a four-dimensional regression problem that is easier to train. However, for this method to perform on cluttered scenes, good scene segmentation is required. A similar keypoint-based representation that encodes the contact points of both fingers along with the grasp center is proposed in [54, 55]

**(Semi-)Implicit grasp prediction.** Implicit models predict a quality value of grasp candidates [13, 56]. PointNet-GPD [14] learns a features space for pointclouds to predict quality of grasps that are sampled in a similar fashion to [36] in scenes. [21] extends PointNetGPD for regressing poses and predicting their qualities. [57] predicts grasping outcomes using a geometry-aware representation that reconstructs the occupancy grid of an object from RGBD input. A coarse-to-fine approach is presented in [23] with a backbone point network proposing grasp points on an object surface, and a refinement step regresses the orientation of grasps for single objects. A multi-scale transformer is introduced in [58] that regresses 7DoF grasps (6DoF grasps and the gripper width) in cluttered scenes, using orientation bins to facilitate learning in  $SE(3)$ . [59] learns a contextual grasp generator with Hough voting [60] and a contextual attention module to perform explicit grasps pose prediction and quality estimation in scenes. [15] follows ideas similar to the contact-based representation [61] and proposes a two-point-based representation for 6DoF grasps that seems effective for detecting grasps object-edges. VGN [22] processes the TSDF of a scene to perform semi-implicit grasp detection (quality prediction in 3D pose and regression of 3D orientation). GIGA [31] extends VGN by training a convolutional occupancy network to reconstruct the scene as an auxiliary task, showing that sharing the features between scene occupancy and grasp prediction improves the primary grasping task. [19, 20] propose learning 6DoF grasps as cost functions on object surfaces to be used in trajectory optimization. The promising results of implicit representation learning [25–27, 29, 28] provide a valuable feature space for robot learning from perception [62, 63]. Recently, the use of NERF [35] was applied for learning grasps of transparent objects for learning a depth representation on to of which grasp can be detected [64, 32].